Supplementary Information

A Multifunctional Self-Healing Binder with Strong Interfacial Interactions and Structural Stability for High-Energy-Density Silicon Anodes

Haeyoung Lee [a†], Jeongmin Lee [a†], Jaewon Lee[a*], Woo-Jin Song [a,b,c,*]

[a] *Department of Chemical Engineering and Applied Chemistry, College of Engineering, Chungnam National University, 99 Daehak-ro (st), Yuseong-gu, Daejeon 34134, Republic of Korea*
[b] *Department of Organic Materials Engineering, College of Engineering, Chungnam National University, 99 Daehak-ro (st), Yuseong-gu, Daejeon 34134, Republic of Korea*
[c] *Institute of Carbon Fusion Technology (InCFT), Chungnam National University, Daejeon, 34134, Republic of Korea*

[*] Corresponding authors.
E-mail addresses: jaewonlee@cnu.ac.kr (Jaewon Lee), wjsong@cnu.ac.kr (W.-J. Song)
[†]These authors contributed equally to this work.

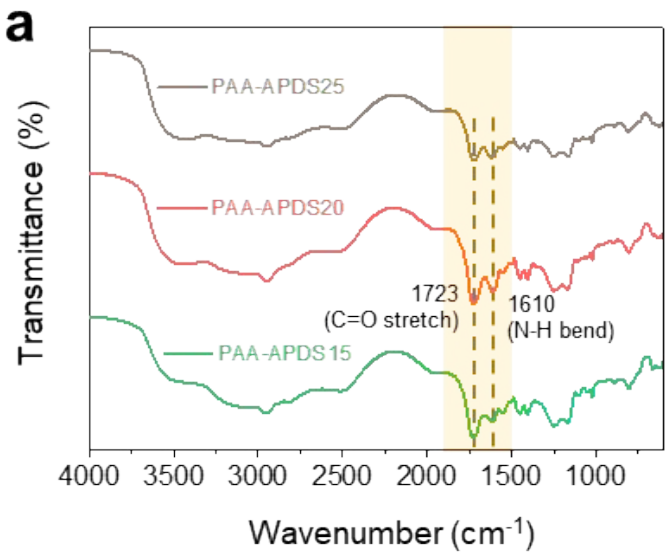

Fig. S1. FT-IR spectra of PAA-APDS15, PAA-APDS20 and PAA-APDS25.

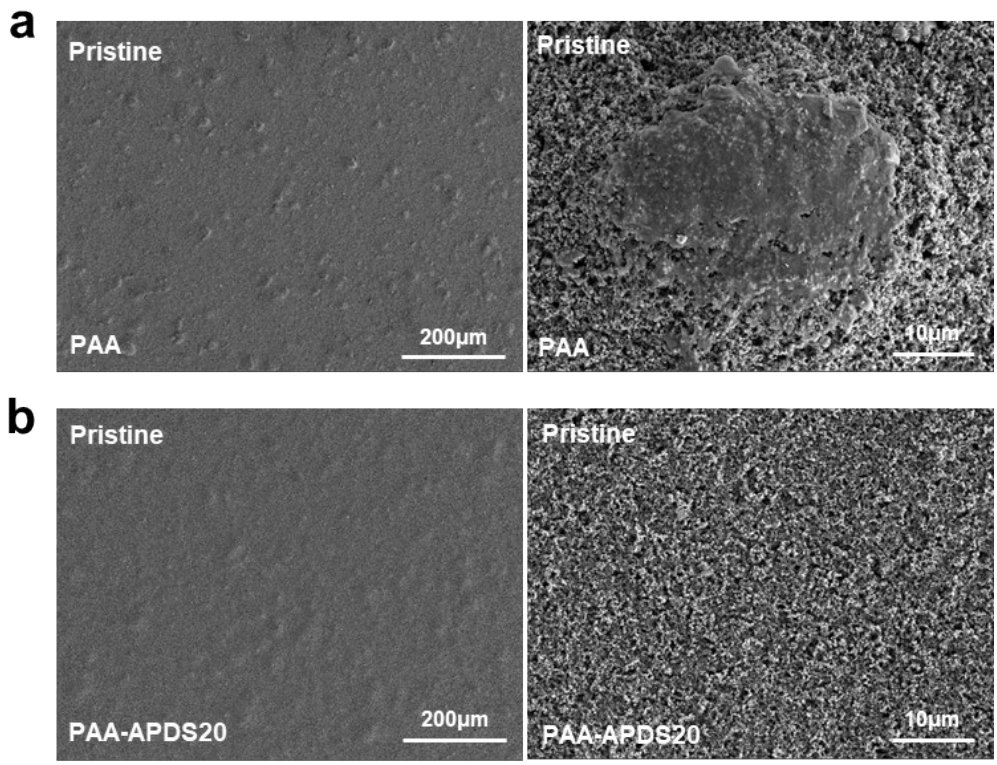

Fig. S2. SEM image of pristine Si electrode surfaces (a) Si/PAA (b) Si/PAA-APDS20.

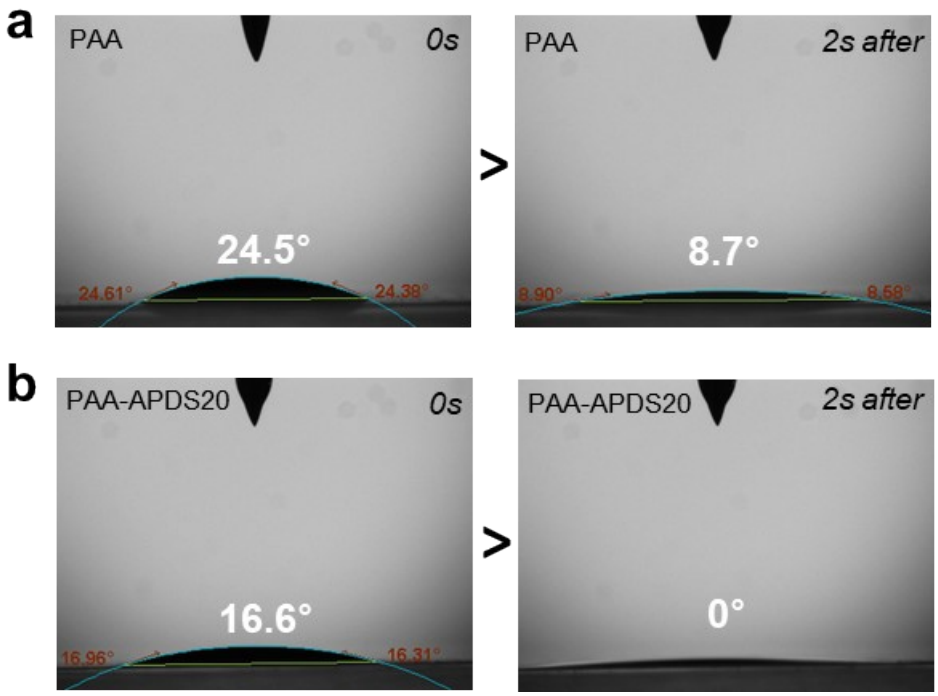

Fig. S3. The contact angles of the Liquid electrolyte with (a) Si/PAA and (b) Si/PAA-APDS20.

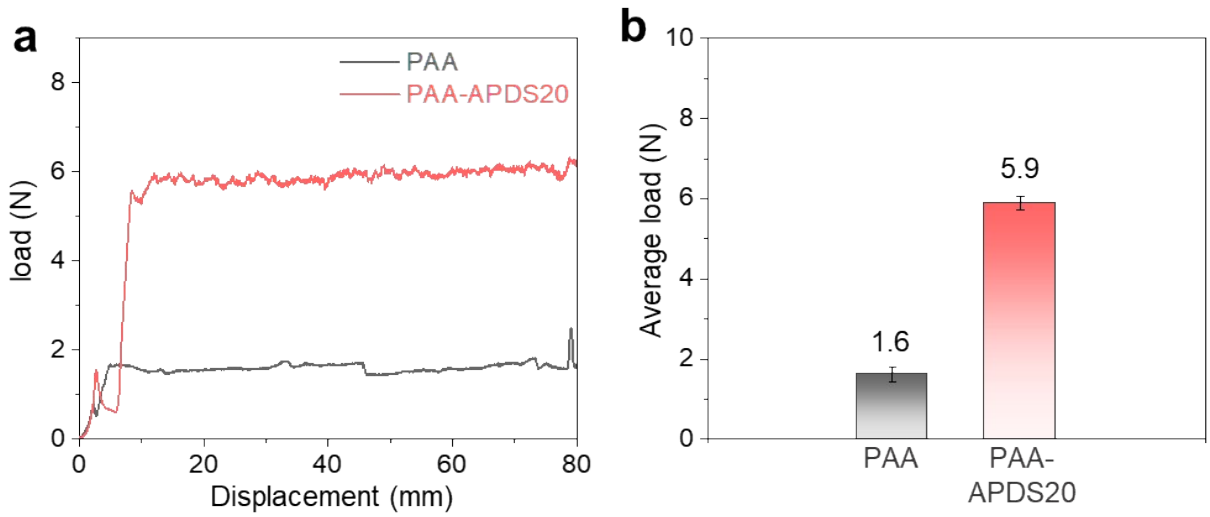

Fig. S4. (a) cross-cut adhesion test of Si electrodes with PAA and PAA-APDS20 binder through 180° peel off test (b) The average graph of peeling strength.

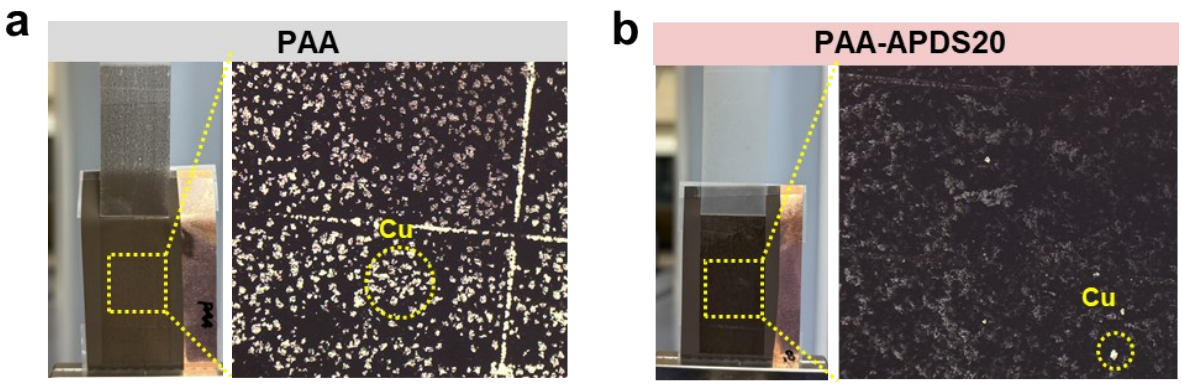

Fig. S5. (a) Photo and optical image of Si electrode with PAA and (b) PAA-APDS20 after cross-cut adhesion test.

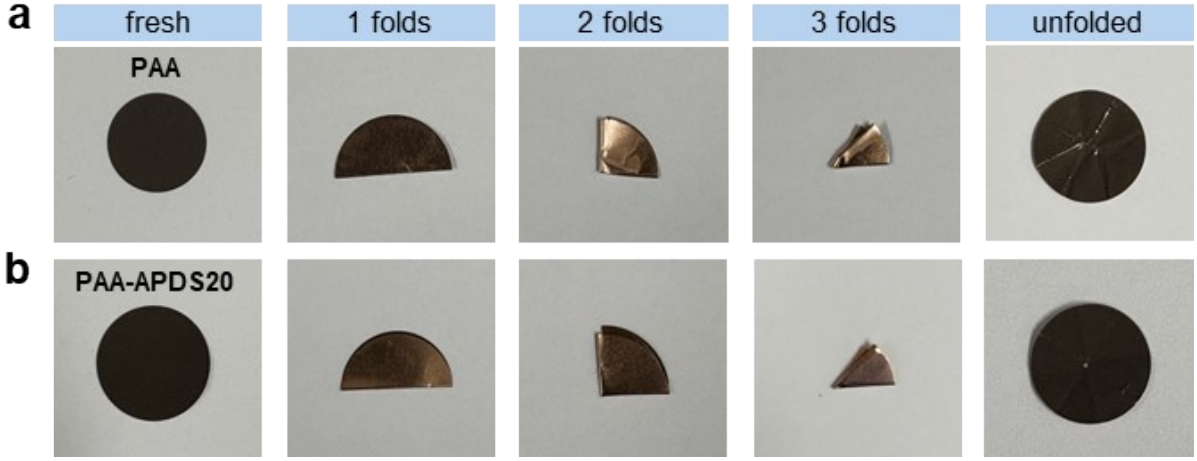

Fig. S6. Folding test of (a) Si electrode with PAA, (b) Si electrode with PAA-APDS20.

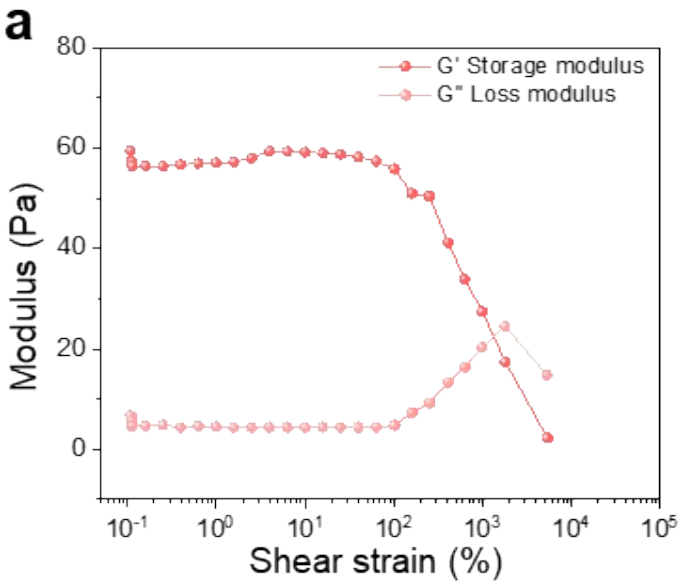

Fig. S7. Rheological characterization of the PAA-APDS20 binder hydrogel by amplitude sweep measurements.

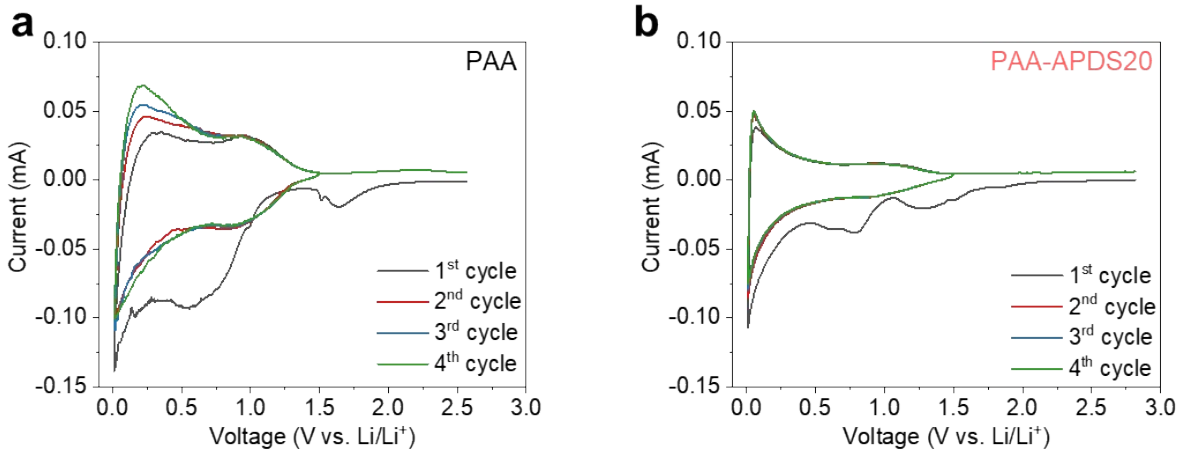

Fig. S8. Cyclic voltammetry (CV) curves of electrodes composed of binder and Super P at a mass ratio of 1:1, measured at a scan rate of 0.1 mV s^{-1}: (a) PAA binder and (b) PAA-APDS20 binder.

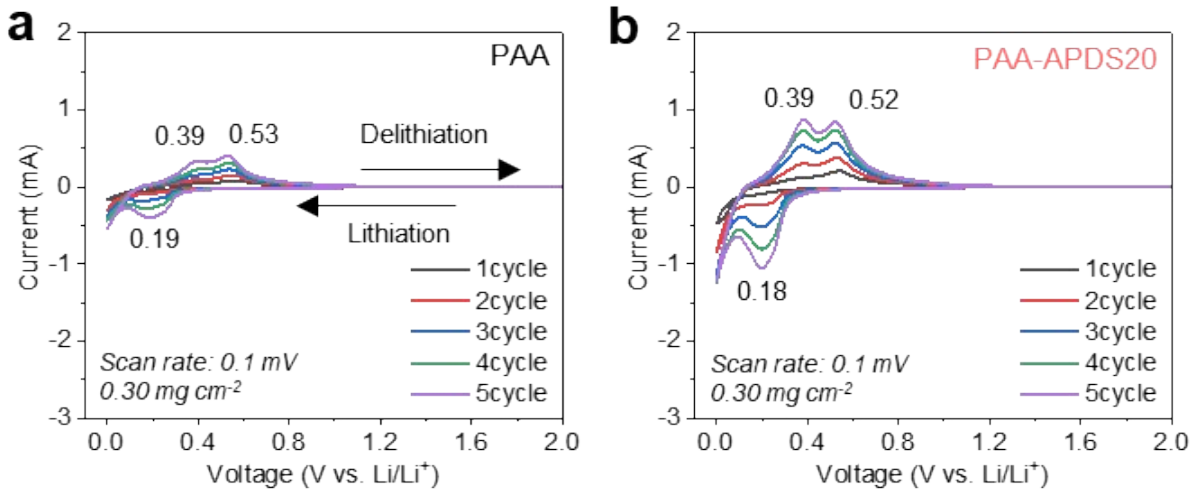

Fig. S9. CV curves of Si anode half-cell (a) with the Si/PAA and (b) Si/PAA-APDS20 binders.

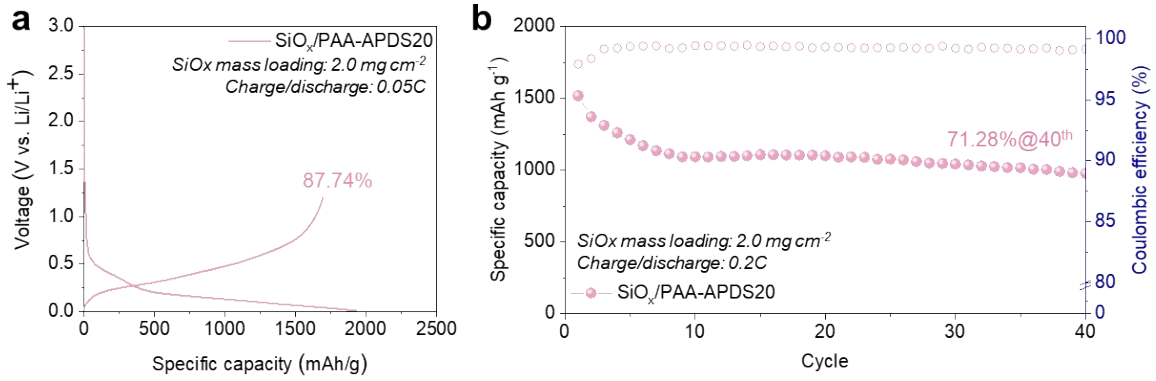

Fig. S10. Electrochemical performance of SiOx anode in high-mass-loading half-cell. (a) Initial voltage profiles of Si anodes with PAA-APDS20 binder. (b) Cycle performance and Coulombic efficiency.

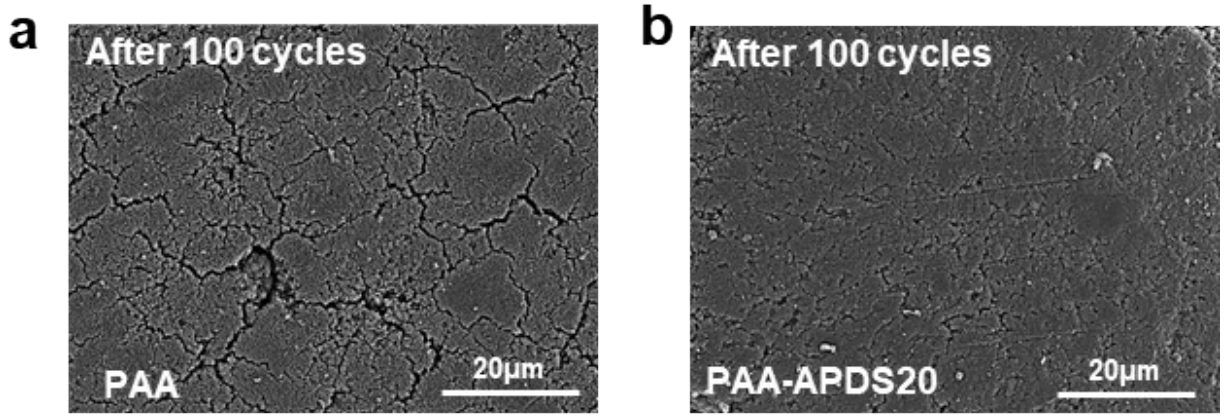

Fig. S11. SEM image of Si anode surfaces after 100 cycles; (a) Si/PAA (b) Si/PAA-APDS20.

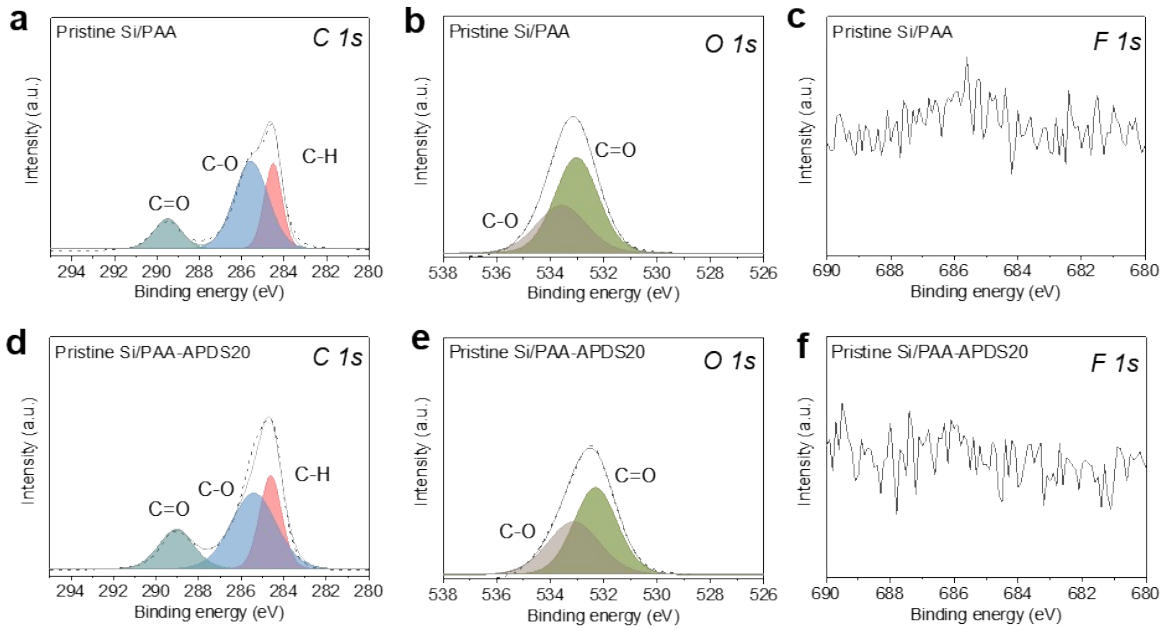

Fig. S12. XPS spectra of C 1s, O 1s, F 1s ; (a-c) spectra of Si/PAA before cycles. (d-f) Si/PAA-APDS20 before cycles.

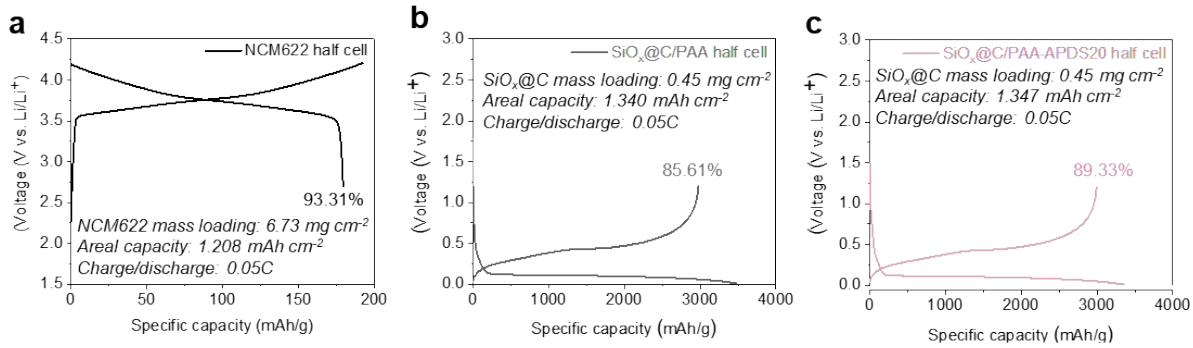

Fig. S13. Initial voltage profiles of half cells (a) NCM622 cathode (b) SiOx@C/PAA anode (c) SiOx@C/PAA-APDS20 anode**.**

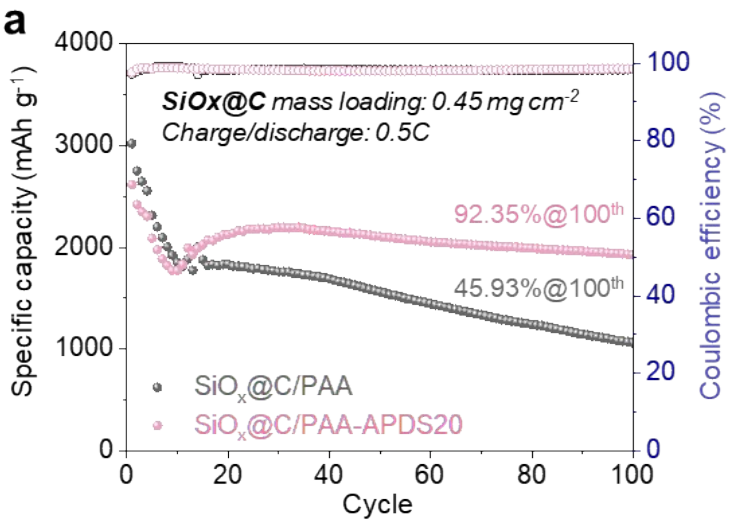

Fig. S14. (a) Cycle performance and Coulombic efficiency of SiOx@C/PAA and SiOx@C/PAA-APDS20 anode half cells.

Sample	C	H	N	O	Crosslink density(%) [a]
PAA	47.56	5.73	0.08	48.48	-
PAA-APDS-15	48.99	7.21	5.37	31.73	16.20
PAA-APDS-20	50.54	7.15	6.10	25.78	21.28
PAA-APDS-25	51.45	7.55	6.90	20.57	27.69

[a] Crosslink density = $(n_{crosslinker})/(n_{PAA}+n_{crosslinker})$

Table S1. Elemental composition (C, H, N, and O) and calculated crosslink density of PAA and PAA-APDS binders with different APDS feed ratios.

Resistance	After 1 cycle		After 100 cycles	
	PAA	PAA-APDS20	PAA	PAA-APDS20
R_s (Ω)	2.79	2.52	5.227	3.55
R_{SEI} (Ω)	11.36	5.78	30.99	16.99
R_{ct} (Ω)	31.75	19.04	31.33	20.74

Table S2. EIS measurements of Si anode (a) with PAA binder and (b) PAA-APDS20 binder.